

Anti-chiral states in twisted graphene multilayers

M. Michael Denner,^{1,2} J. L. Lado,^{3,1} and Oded Zilberberg¹

¹*Institute for Theoretical Physics, ETH Zurich, 8093 Zurich, Switzerland*

²*Department of Physics, University of Zurich, Winterthurerstrasse 190, 8057 Zurich, Switzerland*

³*Department of Applied Physics, Aalto University, 00076 Aalto, Espoo, Finland*

(Dated: April 21, 2022)

The advent of topological phases of matter revealed a variety of observed boundary phenomena, such as chiral and helical modes found at the edges of two-dimensional topological insulators. Anti-chiral states in 2D semimetals, i.e., co-propagating edge modes on opposite edges compensated by a counter-propagating bulk current, are also predicted, but, to date, no realization of such states in a solid state system has been found. Here, we put forward a procedure to realize anti-chiral states in twisted van der Waals multilayers, by combining the electronic Dirac-cone spectra of each layer through the combination of the orbital moiré superstructure, an in-plane magnetic field, and inter-layer bias voltage. In particular, we demonstrate that a twisted van der Waals heterostructure consisting of graphene/(hBN)₂/graphene will show anti-chiral states at in-plane magnetic fields of 8 T, for a rotation angle of 0.2 degrees between the graphene layers. Our findings engender a controllable procedure to engineer anti-chiral states in solid-state systems, as well as in quantum engineered metamaterials.

I. INTRODUCTION

Dirac materials have sparked vast interest in recent years, as their unique electronic properties offer a controllable setting with which to realize new states of matter^{1,2}, as well as engineer topological phenomena^{3,4}. A paradigmatic example of a 2D Dirac material is graphene^{5,6}, whose spectrum exhibits Dirac-like cones at the corners (valleys) K and K' of its hexagonal Brillouin zone. The two inequivalent K and K' valleys have opposite chiralities with associated quantized Berry phase². Correspondingly, in a finite system of zigzag termination, these valleys are connected by topological dispersionless edge states^{7,8}. This flat edge band has been observed experimentally in a variety of systems.^{9–12} Interestingly, such Dirac materials can be considered as ideal starting points for realizing other exotic surface modes,^{7,13–16} by introducing proper perturbations to the Dirac cones.

A paradigmatic example of the versatility of the Dirac system consists of breaking time-reversal symmetry in the honeycomb lattice, and opening up a valley-dependent mass.¹³ In this situation, a topologically non-trivial bulk gap opens at the Dirac points, and the above-mentioned flat edge band develops into the chiral subgap modes of a Chern insulator, where the latter are dispersive and counter-propagating on opposite edges of the 2D material^{17,18}. Even though this state has not been observed in solid-state graphene, its proposal led to generalizations in other materials, such as magnetically-doped topological insulators^{19,20} and twisted bilayer graphene^{21,22}, as well as in engineered emulation of Chern physics in cold atoms^{23,24} and photonics^{25,26}.

A direct generalization of such Dirac spectrum engineering includes a perturbation with a spin- and valley-dependent mass¹⁴, which gives rise to quantum spin Hall insulators. Here, the former flat edge band states develop into helical subgap modes,²⁷ i.e., the bulk spectrum is

gapped, but at each edge a pair of counter-propagating states with opposite spins appear. In graphene, spin-orbit coupling creates a rather small topological gap, making observation of such physics challenging. Analogous physics, however, appear in more complex materials, such as monolayer tungsten ditelluride²⁸.

Interestingly, anti-chiral edge modes appear in systems where the bulk spectrum is not gapped.¹⁶ Here, on opposite edges of the 2D system, the modes propagate in the same direction, compensated by oppositely-dispersive semi-bulk modes. Such anti-chiral states are generated by introducing a valley-dependent energy shift to the Dirac cones, which can be mathematically engineered using tailored long-ranged hopping amplitudes.^{16,29,30} Such hopping is not present in real graphene and, even though anti-chiral states are technically viable, solid-state realizations of them have not been found so far.

In this work, we put forward a mechanism to create anti-chiral states based on graphene multilayers and applied electromagnetic fields. The system's additional layer degrees of freedom brings forth anti-chiral states in a realistic solid state platform through a combination of an applied in-plane magnetic field and inter-layer bias voltage. Thus, Dirac cones of different layers are selectively modified, so that co-propagating edge modes on opposite edges manifest. We first illustrate this idea in aligned bilayer sheets, providing a mechanism that can be readily applied to cold atom setups^{31–33} and artificial Dirac systems.^{34,35} We then extend our proposal to a graphene/(hBN)₂/graphene twisted multilayer, demonstrating that the increased effective lattice constant allows for the creation of anti-chiral states at a magnetic field of 8 T for a 0.2 degrees twist rotation. Our proposal puts forward a viable scheme by which to realize anti-chiral states in twisted van der Waals systems, opening up future experimental studies of anti-chiral systems.

The paper is organized as follows: In Sec. II, we start by illustrating the fundamental mechanism on AB -

stacked bilayer graphene, exploring the impact of in-plane magnetic fields and interlayer bias voltage on both the bulk and edge modes of the system. Specifically, we show that the in-plane magnetic field shifts the Brillouin zones of the two layers relative to one another, such that Dirac cones of different layers can couple in reciprocal space. In this setting, the added interlayer bias voltage tilts the relative energies of the two cones, revealing anti-chiral edge states in a finite system. In section III, we demonstrate that a similar phenomenology happens in a twisted bilayer system, where the emergence of the moiré length dramatically reduces the required magnetic field. Specifically, we show that a graphene/(hBN)₂/graphene twisted multilayer provides a feasible van der Waals system for the creation of anti-chiral states. Finally, in Sec. IV, we summarize our results and provide an outlook to our findings.

II. ANTI-CHIRAL STATES IN *AB*-STACKED GRAPHENE BILAYERS

To illustrate how anti-chiral states can be engineered in a stacked *AB* graphene bilayer, let us first briefly summarize the electronic properties of graphene monolayer and aligned bilayers. Single-layer graphene is a hexagonal two-dimensional material with two atoms (denoted *A* and *B*) per unit cell. As the atoms are identical (carbon), its energy spectrum exhibits massless Dirac-cone band touchings at the six corners of its hexagonal Brillouin zone. The cones appear in pairs with opposite chiralities at the so-called *K* and *K'* valleys.² At a proper termination of the graphene system, e.g., at a zig-zag termination, flat edge bands spectrally connect the two valleys. Using a coupled-wire description of the 2D system, these edge bands can be understood to be made of uncoupled 0D bound modes of 1D topological insulators⁸. Including a sublattice dependent second-neighbor hopping,¹⁶ the Dirac cones can be shifted in energy, turning the topological flat bands into anti-chiral states. However, real graphene monolayers do not host such long-ranged hopping and the Dirac cones are located at the same energy. As a result, such a valley-dependent energy shift must be artificially engineered.

Graphene bilayers can provide a possible platform to engineer valley-dependent energy shifts. They consist of two coupled graphene monolayers that can be arranged in three main configurations: *AA*, *AB*, and twisted stacking. In the following, we start by considering *AB*-stacked graphene, in which an atom of the *B*₁ sublattice is directly situated above an atom of the *A*₂ sublattice, where 1 and 2 denote top and bottom layers, respectively. The remaining *A*₁ and *B*₂ lie at the center of the honeycombs formed by the complementary layer, see Fig. 1(a). The unit cell of the *AB*-stacked bilayer therefore contains 4 atoms. Similarly to single-layer graphene, the corresponding low-energy spectrum exhibits six band touchings divided into two inequivalent valleys. Con-

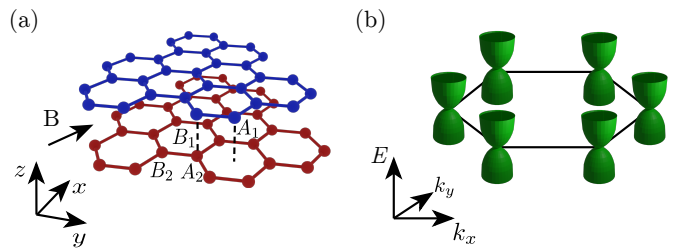


FIG. 1. *AB*-stacked bilayer graphene. (a) Real space lattice of *AB*-stacked bilayer graphene, consisting of two graphene sheets that are shifted with respect to each other, while being aligned only at two points of the unit cell. (b) Corresponding schematic low-energy spectrum in the hexagonal Brillouin zone. The combination of the two graphene sheets results in a quadratic low-energy bandstructure, appearing at the six corners of the first Brillouin zone.

trary to the graphene monolayer, the spectrum in these valleys is not linear, but displays a quadratic dispersion, see Fig. 1(b)^{36,37}. We can intuitively understand this difference: In the absence of interlayer tunnel coupling, the system has four Dirac cones (two per layer and two per valley). The interlayer coupling hybridizes the *B*₁ and *A*₂ orbitals and repels states from half-filling, leading to high energy bands. The states localized at the uncoupled *A*₁ and *B*₂ sites remain uncoupled and generate the low-energy quadratic touching points. In this bilayer case, Dirac cones between different layers can be shifted in energy simply by applying a bias between the layers, yet the already existing hybridization between cones gives rise to a gap opening³⁸ and the emergence of a quantum valley Hall state.³⁹ In the following, we will show how this gapping out of all the Dirac cones is avoided by creating momentum shifts with applied in-plane magnetic fields.

Applying an in-plane magnetic field between the two graphene layers modifies the quasimomentum of each graphene layer, and is described by the minimal coupling $\mathbf{p} \rightarrow \mathbf{p} - \mathbf{A}$. The vector potential \mathbf{A} incorporates the magnetic field, which can, for a general in-plane field with orientation ϕ , be written as $\mathbf{B} = B(\sin(\phi), \cos(\phi), 0)^T$ with $\mathbf{A} = B(\cos(\phi)z, -\sin(\phi)z, 0)^T$. Choosing the coordinate origin to coincide with a lattice site of the lower layer, we obtain that only the quasimomentum in the upper layer is affected by the in-plane magnetic field. This implies that the in-plane electron momentum in the upper layer is changed by the external field according to $\mathbf{p} \rightarrow \mathbf{p} + \Delta\mathbf{p}$ with $\Delta\mathbf{p} = Bd(-\cos(\phi), \sin(\phi), 0)^T$, where d is the distance between the two layers. Equivalently, this can be understood as a momentum kick by a Lorentz force acting on electrons tunnelling between the two layers⁴⁰. This causes the quadratic spectrum to separate back into Dirac cones of the upper and lower layer^{40,41}, which are now shifted in momentum with respect to each other, see Fig. 2(a). The separation of the Brillouin zones of the two layers is proportional to the

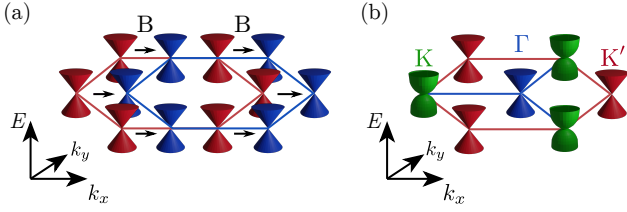


FIG. 2. *AB*-stacked graphene subject to an in-plane magnetic field. (a) Schematic depiction of the low-energy band-structure in the first Brillouin zone for (a) a small in-plane magnetic field B and (b) a large B that hybridizes the cones once more. The Lorentz force acting on electrons tunneling between the two graphene layers causes a momentum separation between the lower (red) and upper (blue) layer spectra [arrows in (a)], thus effectively decoupling the layer Dirac cone spectra from one another. A strong in-plane magnetic field is able to merge Dirac cones by re-combining different valleys, thus selectively producing quadratic spectra at the merged points, while separating the bandstructures of the layers in other parts of the Brillouin zone.

strength B and depends on the orientation ϕ of the applied magnetic field.

As the Dirac cones are shifted with respect to each other, the possibility arises to merge them once more at specific angles and field strengths. An interesting situation occurs for a field strength of $B = \frac{1}{ad} \frac{4\pi}{3\sqrt{3}}$, where a is the lattice constant and d the layer spacing. Here, the field strength corresponds to the distance between opposite valleys in the hexagonal Brillouin zone. Thus, only one pair of valleys from the two layers is merged, whereas the other valley pair remains separate, see Fig. 2(b). Correspondingly, the merged valleys exhibit quadratic dispersion band touchings as in the *AB*-stacked case, while the valleys that are not merged exhibit linear Dirac cones as in a monolayer graphene. At the corners of the hexagonal Brillouin zone, the latter are formed by the lower layer that is unaffected by the magnetic field. At the Γ -point, the shifted upper layer's Dirac cone appears.

The effect of the magnetic field can be incorporated into a tight-binding description of the system using Peierls' substitution, i.e., by modifying the hopping amplitudes as

$$t_{ij} \rightarrow t_{ij} e^{i\Phi_{ij}} = t_{ij} e^{i \int_{\mathbf{r}_i}^{\mathbf{r}_j} \mathbf{A} \cdot d\mathbf{r}}, \quad (1)$$

where \mathbf{A} is the vector potential, $\mathbf{r}_{i,j}$ are the positions of the atoms in the material, and t_{ij} is the bare hopping amplitude between electron valence orbits on atoms i and j . We, thus, write down the tight-binding Hamiltonian for *AB*-stacked graphene^{36,37} in the presence of an in-plane magnetic field, and obtain the corresponding spectrum, see Fig. 3(a). Similar to the effective low-energy description in Fig. 2, the in-plane magnetic field clearly separates the bandstructures of the two layers in certain areas of reciprocal space. In the non-merged valley at the Γ -point, the spectrum originates from isolated monolayers, whereas the merged valley exhibits a quadratic dispersion

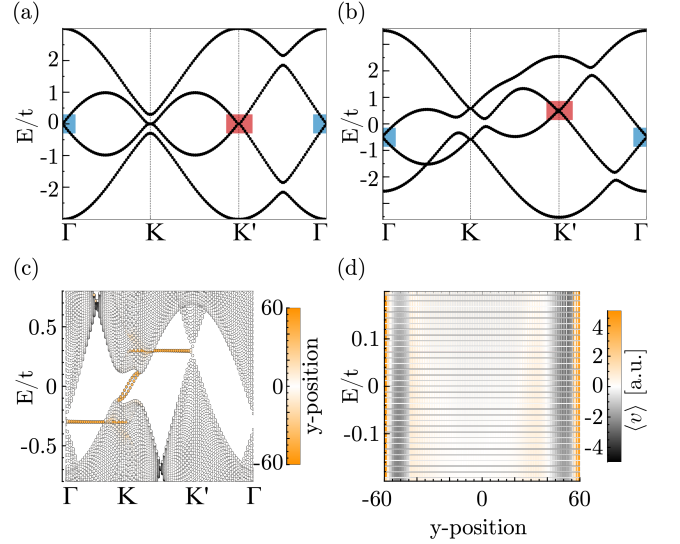


FIG. 3. Bandstructure of *AB*-stacked bilayer graphene. (a) The spectrum with an in-plane magnetic field that merges Dirac cones from different layers at the K -points (quadratic touching), and leaves linear uncoupled Dirac cones at the Γ - and K' -points (marked by blue and red squares), cf. Fig. 2. (b) Since the quadratic touching points are formed by states originating from different layers, an interlayer voltage bias gaps them. Moreover, the bias voltage shifts in energy the Dirac cones of the upper and lower layers relative to one another. (c) This procedure reveals anti-chiral edge states when considering a finite system of 20 unit cells with zigzag termination, with the color-map indicating the position of eigenstates along the finite dimension. (d) The anti-chiral states propagate in the same direction along the boundary (orange) compensated by a bulk current (black) of opposite direction close to the edge, as can be seen by the spatially resolved group velocity.

caused by interlayer coupling.

By applying a bias voltage between the stacked layers, the energy of the states in each layer are shifted with respect to one another (inducing layer polarization), and a gap opens up at the quadratic touching points^{42–44}. As a consequence, in standard *AB*-stacked graphene with $B = 0$, the system is fully gapped, as the states forming the quadratic touching points are split off. Introducing an in-plane magnetic field $B \neq 0$, a similar behaviour is obtained at the merged valley, where the quadratic dispersion is replaced by a band gap, which is tunable by the strength of the induced layer polarization, see Fig. 3(b). At the same time, since the in-plane field decoupled the spectra of the two layers at the Γ - and K' -points, the full system is not gapped, but instead, the Dirac cone originating from the upper layer is shifted opposite in energy to the Dirac cone of the lower layer. In turn, this means that the system is no longer a semimetal, but it becomes a conductor, as there is a finite density of states crossing at any filling of the material.

Interestingly, at half-filling, the bulk becomes conducting with a bulk current that is compensated by co-

propagating edge modes. The latter anti-chiral states are revealed in a finite system, see Fig. 3(c). A special feature of graphene is that these edge modes emerge only in certain geometries, for example in bilayer graphene nanoribbons with zigzag edges^{8,45–47}. Specifically, in our case, a finite bilayer system with zigzag termination [Fig. 3(c)] shows flat edge bands connecting the Dirac cones of each layer that are then forced to disperse due to the shifted energy between the layers. To ensure charge neutrality, this flow of charge carriers at the boundary is compensated by a bulk current flowing in the opposite direction, see Fig. 3(d). This is reflected in the bulk bands crossing half-filling at the not-merged valleys at the Γ - and K' -points.

We thus obtain a scenario that generates anti-chiral states in a realistic system, using the tunability offered by the application of magnetic and electric fields on bilayer systems. Note that the key ingredient of shifted Dirac cones that drag in energy the topological flat edge bands manifests here in similitude to the case of the modified Haldane model¹⁶. Furthermore, we can reverse the propagation direction of these anti-chiral states by either changing the sign of the layer polarization, or by using an opposite field to merge the Dirac cones at the K' -valley. However, the in-plane magnetic field required to shift the stacked graphene Brillouin zones with respect to each other for a real graphene bilayer corresponds to an unrealistically large value, $B = \frac{1}{ad} \frac{4\pi}{3\sqrt{3}} = 19.6$ kT, where we converted to real units by taking $a = 2.46$ Å³⁶ and $d = 3.3$ Å⁴⁰. Nevertheless, it is important to emphasize that such large effective fields can be achieved in quantum engineered systems, where synthetic gauge fields can be induced^{26,48}. As in this work we are ultimately interested in showing how to create anti-chiral states in solid state materials, in the following, we show how an analogous mechanism can be realized in twisted bilayer graphene, dramatically lowering the required magnetic fields.

III. ANTI-CHIRAL STATES IN TWISTED BILAYER GRAPHENE

In the previous section, we saw that the AB -stacked bilayer graphene exhibits anti-chiral states once two coupled Dirac cones are shifted in energy relative to one another. Yet, the in-plane magnetic field required for selective coupling of these Dirac cones was too large, a feature simply related with the lattice constant and layer spacing associated with such a momentum space translation. Hence, in this section, we move to investigate a similar scenario in twisted bilayer graphene, in which the emergence of a new moiré length will dramatically lower the magnetic field required. In such a system, the two graphene layers are not perfectly aligned, but form a relative angle, creating a so-called moiré superstructure⁴⁹. This causes an alternating pattern of AB , AA and BA stackings, resulting in a supercell up to 1000 times larger than in a graphene monolayer, see Fig. 4(a).

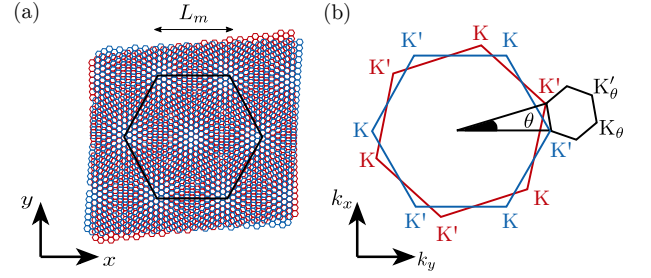


FIG. 4. Twisted bilayer graphene. (a) Real space moiré pattern formed by the relative rotation of two graphene layers (red and blue mark atoms in the lower and upper layers). (b) Corresponding Brillouin zones of the lower (red) and upper (blue) layer rotated by angle θ . The superstructure in real space of length L_m induces a much smaller Brillouin zone in reciprocal space.

Such moiré patterns are observed with scanning tunneling spectroscopy⁵⁰, and the period is described as⁴⁹

$$L_M = \frac{a}{2 \sin \frac{\theta}{2}} \approx \frac{1}{\theta}, \quad (2)$$

such that the size of the unit cell scales roughly as $\frac{1}{\theta}$ for small twisting angles θ . The corresponding first Brillouin zone is again hexagonal, but considerably smaller than that of a normal graphene layer, see Fig. 4(b).⁴⁹ Correspondingly, this yields a reduced inter-Dirac cone reciprocal distance

$$\Delta K = |\mathbf{K}_\theta - \mathbf{K}'_\theta| = \frac{4\pi}{3a} \sqrt{2\sqrt{1 - \cos \theta}}. \quad (3)$$

Hence, for small twisting angles, the twist dramatically reduces the distance between the Dirac valleys, i.e., this allows for much smaller in-plane magnetic fields necessary for the generation of selective Dirac cone coupling and the appearance of anti-chiral states, cf. section above.

The tight-binding Hamiltonian describing the twisted bilayer graphene in the presence of in-plane magnetic fields can be written as^{51–54}

$$H = \sum_{\langle i,j \rangle} t(\Phi, \mathbf{r}_i, \mathbf{r}_j) c_i^\dagger c_j + \sum_{i,j} \hat{t}_\perp(\Phi, \mathbf{r}_i, \mathbf{r}_j) c_i^\dagger c_j + \Delta \sum_i \tau_z^{ii} c_i^\dagger c_i. \quad (4)$$

The first term describes nearest-neighbor $\langle i,j \rangle$ hopping within the layers, with the hopping amplitude t modified by Peierls' substitution (1). The hopping between the twisted layers $\hat{t}_\perp(\Phi, \mathbf{r}_i, \mathbf{r}_j)$ depends on the relative distance between the atoms on different layers, and has its maximum value t_\perp for perfect stacking. The last term describes the bias-voltage induced layer polarization. We denote $\Phi = Bad$, to be the flux piercing the interlayer plaquette. As a reference, in graphene the parameters are³⁶ $t = 3$ eV and $t_\perp = 300$ meV. Similar to the aligned AB -stacked case in the previous section,

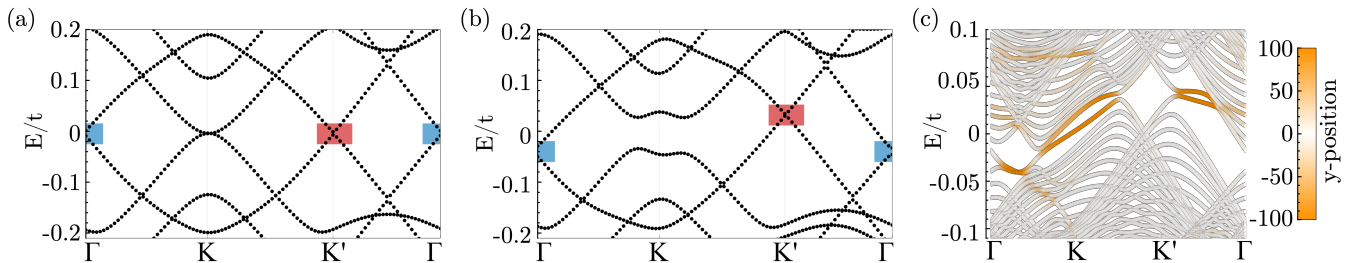


FIG. 5. Bandstructure of twisted bilayer graphene in the anti-chiral regime. (a) In the presence of an in-plane magnetic field that selectively merges Dirac cones from different layers, cf. Figs. 2 and 3, the in-plane magnetic field reduces the number of Dirac cones by creating quadratic touching points in the merged valley. (b) An applied interlayer bias voltage opens a gap at the quadratic touching points and shifts the unpaired Dirac cones from the different layers relative to one another (red and blue squares). (c) Anti-chiral edge states appear when considering a finite system, with the colormap indicating the position of the eigenstates along the finite dimension. It is observed that the states localized on opposite edges propagate in the same direction, as expected from anti-chiral modes. This regime is achieved in the twisted graphene/(hBN)₂/graphene heterostructure for a rotation angle of 0.2 degrees and an in-plane magnetic field of 8 T.

the in-plane magnetic field causes the energy spectrum to separate into two cones per valley, which are shifted by the applied field⁵⁵. This means that their separation can be controlled by the angle ϕ and strength B of the field. As a reference, the distance between the cones can be bridged by a field of $\Phi \approx 0.02$ in natural units, corresponding to a magnetic field of $B = 162.2$ T, which is beyond experimentally feasible values.

On the bright side, by exploiting twist engineering, we have dramatically reduced the magnetic field required to merge the Dirac points in twisted graphene bilayers. Nevertheless, the field strength required is still too large for a feasible realization of anti-chiral states in twisted bilayer graphene at angles above 1 degree. A simple recipe to bring down the required fields is to increase the flux associated to a certain rotation angle, or to decrease the interlayer hopping to conserve the Dirac cones at smaller rotation angles. Luckily, both schemes can be achieved by including a thin hBN insulating layer between the twisted graphene layers, where the effective hopping between the layers in the resulting graphene/hBN/graphene heterostructures can be tuned between 2–70 meV when inserting 3–1 hBN layers.⁵⁶ In particular, taking two layers of hBN as spacers brings the effective interlayer hopping t_{\perp} to 20 meV,⁵⁶ while preserving the original Dirac cones spectra up to rotation angles of 0.1 degrees.^{51,53,57} Furthermore, the inclusion of two hBN layers increases the interlayer distance by a factor of 3 approximately.⁵⁶ Taking this into account, we obtain that a twisted heterostructure graphene/(hBN)₂/graphene would show anti-chiral states for an angle of 0.2 degrees rotation and a magnetic field of 8 T, which is an experimentally achievable regime. This demonstrates that anti-chiral states can be realistically engineered in twisted graphene/hBN superlattices, opening up a feasible solid state platform for anti-chiral physics.

We now explicitly show that anti-chiral states indeed emerge in the effective model for twisted bilayer graphene. We directly focus on the regime in which

the magnetic flux associated is comparable with the lattice constant, where for computational convenience we use a rescaling trick.⁵⁸ In this situation, the number of Dirac cones can be reduced by merging opposite graphene valleys by applying the required in-plane magnetic flux [Fig. 5(a)], which will be 8 T for the graphene/(hBN)₂/graphene heterostructure at a rotation angle of 0.2 degrees. In order to realize anti-chiral states, the two remaining Dirac cones are shifted in energy relative to one another. This is again achieved by adding an interlayer bias voltage [Fig. 5(b)], i.e., on-site energies Δ that have a different sign $\tau_z^{ii} = \pm 1$ depending on the corresponding layer. This causes the separated Dirac cones of the upper and lower layer to be shifted in energy, whereas the quadratic merging point is gapped out. At the gapped merging point, anti-chiral edge states appear. Since the remaining cones are shifted up and down in energy, bulk states are present at the same chemical potential that compensate the co-propagating edge channels [Fig. 5(b)]. The system is no longer insulating, but metallic, with currents along the edges propagating opposite to the bulk flow [Fig. 5(c)]. To summarize, anti-chiral states can be obtained in a twisted bilayer graphene system using the same recipe of applying in-plane magnetic and interlayer electric fields.

We recall that in the *AB*-stacked model in Sec. II, the direction of the anti-chiral states could be reversed by either changing the sign of the gap opening bias, or by reversing the field direction. Interestingly, applying such a modification in the twisted case shows no change in the propagation direction. This is because of the lack of rotational symmetry of the twisted layers. Changing the signs of the on-site potentials effectively corresponds to rotating the graphene sheets around an in-plane axis, thus also changing the direction of the currents along the edges. In a normal *AA*- or *AB*-stacking, this produces the same crystal structure, with reversed layer polarization. In contrast, in twisted bilayer graphene, the angle between the two layers destroys this symmetry, such

that a rotation creates a new structure, possessing identical current directions. The direction of the currents can however still be reversed by the time-reversal breaking direction, which corresponds to an inversion of the magnetic field. This means merging Dirac cones in a different valley. Since these valleys are related by time-reversal symmetry, the propagation direction is reversed.

IV. CONCLUSIONS

To summarize, we put forward a procedure to create anti-chiral states in graphene multilayer systems, by combining magnetic fields and interlayer bias. In particular, we have demonstrated that a twisted graphene/(hBN)₂/graphene heterostructure at 0.2 degrees rotation will show anti-chiral states for in-plane magnetic fields of 8 T. This fundamental idea consists of engineering a system hosting two Dirac points that can be shifted in energy by means of an interlayer bias. This is achieved by shifting the Dirac cones by an in-plane magnetic field, with the regime being reached when

the in-plane magnetic flux is comparable with the moiré length. Besides a realistic van der Waals solid-state realization, we have proposed also a minimal system consisting of aligned graphene honeycomb lattices in which anti-chiral states can be created. Such a minimal scheme can be exploited in cold atom gases and engineered quantum systems. Our work therefore marks a promising step towards the realization and engineering of these special anti-chiral states, providing a stepping stone towards further studies in anti-chiral metals.

V. ACKNOWLEDGEMENTS

We acknowledge financial support from the Swiss National Science Foundation through grants (PP00P2.1163818 and PP00P2.190078). The authors are grateful to F. Goerg, T. Wolf and I. Petrides for helpful suggestions and fruitful discussions. J.L.L. acknowledges the computational resources provided by the Aalto Science-IT project.

-
- ¹ T. Wehling, A. Black-Schaffer, and A. Balatsky, *Advances in Physics* **63**, 1 (2014).
 - ² A. H. Castro Neto, F. Guinea, N. M. R. Peres, K. S. Novoselov, and A. K. Geim, *Rev. Mod. Phys.* **81**, 109 (2009).
 - ³ Y. Hatsugai, *Journal of Physics: Conference Series* **334**, 012004 (2011).
 - ⁴ M. Z. Hasan and C. L. Kane, *Rev. Mod. Phys.* **82**, 3045 (2010).
 - ⁵ W. Choi, I. Lahiri, R. Seelaboyina, and Y. S. Kang, *Critical Reviews in Solid State and Materials Sciences* **35**, 52 (2010).
 - ⁶ K. S. Novoselov, A. K. Geim, S. V. Morozov, D. Jiang, Y. Zhang, S. V. Dubonos, I. V. Grigorieva, and A. A. Firsov, *Science* **306**, 666 (2004).
 - ⁷ L. Brey and H. A. Fertig, *Phys. Rev. B* **73**, 235411 (2006).
 - ⁸ P. Delplace, D. Ullmo, and G. Montambaux, *Phys. Rev. B* **84**, 195452 (2011).
 - ⁹ C. Tao, L. Jiao, O. V. Yazyev, Y.-C. Chen, J. Feng, X. Zhang, R. B. Capaz, J. M. Tour, A. Zettl, S. G. Louie, H. Dai, and M. F. Crommie, *Nature Physics* **7**, 616 (2011).
 - ¹⁰ G. Z. Magda, X. Jin, I. Hagymási, P. Vancsó, Z. Osváth, P. Nemes-Incze, C. Hwang, L. P. Biró, and L. Tapasztó, *Nature* **514**, 608 (2014).
 - ¹¹ S. Wang, L. Talirz, C. A. Pignedoli, X. Feng, K. Müllen, R. Fasel, and P. Ruffieux, *Nature Communications* **7** (2016), 10.1038/ncomms11507.
 - ¹² O. Gröning, S. Wang, X. Yao, C. A. Pignedoli, G. B. Barin, C. Daniels, A. Cupo, V. Meunier, X. Feng, A. Narita, K. Müllen, P. Ruffieux, and R. Fasel, *Nature* **560**, 209 (2018).
 - ¹³ F. D. M. Haldane, *Phys. Rev. Lett.* **61**, 2015 (1988).
 - ¹⁴ C. L. Kane and E. J. Mele, *Phys. Rev. Lett.* **95**, 226801 (2005).
 - ¹⁵ J. Lado, N. García-Martínez, and J. Fernández-Rossier, *Synthetic Metals* **210**, 56 (2015).
 - ¹⁶ E. Colomés and M. Franz, *Phys. Rev. Lett.* **120**, 086603 (2018).
 - ¹⁷ D. J. Thouless, M. Kohmoto, M. P. Nightingale, and M. den Nijs, *Phys. Rev. Lett.* **49**, 405 (1982).
 - ¹⁸ T. Oka and H. Aoki, *Phys. Rev. B* **79**, 081406 (2009).
 - ¹⁹ R. Yu, W. Zhang, H.-J. Zhang, S.-C. Zhang, X. Dai, and Z. Fang, *Science* **329**, 61 (2010).
 - ²⁰ C.-Z. Chang, W. Zhao, D. Y. Kim, H. Zhang, B. A. Assaf, D. Heiman, S.-C. Zhang, C. Liu, M. H. W. Chan, and J. S. Moodera, *Nature Materials* **14**, 473 EP (2015).
 - ²¹ A. L. Sharpe, E. J. Fox, A. W. Barnard, J. Finney, K. Watanabe, T. Taniguchi, M. A. Kastner, and D. Goldhaber-Gordon, *Science* **365**, 605 (2019).
 - ²² M. Serlin, C. L. Tschirhart, H. Polshyn, Y. Zhang, J. Zhu, K. Watanabe, T. Taniguchi, L. Balents, and A. F. Young, *Science* **367**, 900 (2019).
 - ²³ G. Jotzu, M. Messer, R. Desbuquois, M. Lebrat, T. Uehlinger, D. Greif, and T. Esslinger, *Nature* **515**, 237 EP (2014).
 - ²⁴ N. Fläschner, B. Rem, M. Tarnowski, D. Vogel, D.-S. Lühmann, K. Sengstock, and C. Weitenberg, *Science* **352**, 1091 (2016).
 - ²⁵ M. C. Rechtsman, J. M. Zeuner, Y. Plotnik, Y. Lumer, D. Podolsky, F. Dreisow, S. Nolte, M. Segev, and A. Szameit, *Nature* **496**, 196 (2013).
 - ²⁶ T. Ozawa, H. M. Price, A. Amo, N. Goldman, M. Hafezi, L. Lu, M. C. Rechtsman, D. Schuster, J. Simon, O. Zilberberg, and I. Carusotto, *Rev. Mod. Phys.* **91**, 015006 (2019).
 - ²⁷ M. König, H. Buhmann, L. W. Molenkamp, T. Hughes, C.-X. Liu, X.-L. Qi, and S.-C. Zhang, *Journal of the Physical Society of Japan* **77**, 031007 (2008).

- ²⁸ S. Wu, V. Fatemi, Q. D. Gibson, K. Watanabe, T. Taniguchi, R. J. Cava, and P. Jarillo-Herrero, *Science* **359**, 76 (2018).
- ²⁹ M. Vila, N. T. Hung, S. Roche, and R. Saito, *Phys. Rev. B* **99**, 161404 (2019).
- ³⁰ D. Bhowmick and P. Sengupta, *Phys. Rev. B* **101**, 195133 (2020).
- ³¹ H. M. Price, O. Zilberberg, T. Ozawa, I. Carusotto, and N. Goldman, *Phys. Rev. Lett.* **115**, 195303 (2015).
- ³² T. Ozawa, H. M. Price, N. Goldman, O. Zilberberg, and I. Carusotto, *Phys. Rev. A* **93**, 043827 (2016).
- ³³ L. Tarruell, D. Greif, T. Uehlinger, G. Jotzu, and T. Esslinger, *Nature* **483**, 302 (2012).
- ³⁴ S. Wang, D. Scarabelli, L. Du, Y. Y. Kuznetsova, L. N. Pfeiffer, K. W. West, G. C. Gardner, M. J. Manfra, V. Pellegrini, S. J. Wind, and A. Pinczuk, *Nature Nanotechnology* **13**, 29 (2017).
- ³⁵ K. K. Gomes, W. Mar, W. Ko, F. Guinea, and H. C. Manoharan, *Nature* **483**, 306 (2012).
- ³⁶ E. McCann and M. Koshino, *Reports on Progress in Physics* **76**, 056503 (2013).
- ³⁷ A. Rozhkov, A. Sboychakov, A. Rakhmanov, and F. Nori, *Physics Reports* **648**, 1 (2016).
- ³⁸ E. V. Castro, K. S. Novoselov, S. V. Morozov, N. M. R. Peres, J. M. B. L. dos Santos, J. Nilsson, F. Guinea, A. K. Geim, and A. H. C. Neto, *Phys. Rev. Lett.* **99**, 216802 (2007).
- ³⁹ Z. Qiao, W.-K. Tse, H. Jiang, Y. Yao, and Q. Niu, *Phys. Rev. Lett.* **107**, 256801 (2011).
- ⁴⁰ S. S. Pershoguba and V. M. Yakovenko, *Phys. Rev. B* **82**, 205408 (2010).
- ⁴¹ M. Van der Donck, F. M. Peeters, and B. Van Duppen, *Phys. Rev. B* **93**, 115423 (2016).
- ⁴² E. McCann and V. I. Fal'ko, *Phys. Rev. Lett.* **96**, 086805 (2006).
- ⁴³ E. McCann, *Phys. Rev. B* **74**, 161403 (2006).
- ⁴⁴ H. Min, B. Sahu, S. K. Banerjee, and A. H. MacDonald, *Phys. Rev. B* **75**, 155115 (2007).
- ⁴⁵ K. Nakada, M. Fujita, G. Dresselhaus, and M. S. Dresselhaus, *Phys. Rev. B* **54**, 17954 (1996).
- ⁴⁶ M. Fujita, K. Wakabayashi, K. Nakada, and K. Kusakabe, *Journal of the Physical Society of Japan* **65**, 1920 (1996), <https://doi.org/10.1143/JPSJ.65.1920>.
- ⁴⁷ W. Yao, S. A. Yang, and Q. Niu, *Phys. Rev. Lett.* **102**, 096801 (2009).
- ⁴⁸ I. Bloch, J. Dalibard, and W. Zwerger, *Rev. Mod. Phys.* **80**, 885 (2008).
- ⁴⁹ A. V. Rozhkov, A. O. Sboychakov, A. L. Rakhmanov, and F. Nori, *Phys. Rev. B* **95**, 045119 (2017).
- ⁵⁰ R. Zhao, Y. Zhang, T. Gao, Y. Gao, N. Liu, L. Fu, and Z. Liu, *Nano Research* **4**, 712 (2011).
- ⁵¹ J. M. B. Lopes dos Santos, N. M. R. Peres, and A. H. Castro Neto, *Phys. Rev. Lett.* **99**, 256802 (2007).
- ⁵² A. O. Sboychakov, A. L. Rakhmanov, A. V. Rozhkov, and F. Nori, *Phys. Rev. B* **92**, 075402 (2015).
- ⁵³ E. Suárez Morell, J. D. Correa, P. Vargas, M. Pacheco, and Z. Barticevic, *Phys. Rev. B* **82**, 121407 (2010).
- ⁵⁴ T. M. R. Wolf, J. L. Lado, G. Blatter, and O. Zilberberg, *Phys. Rev. Lett.* **123**, 096802 (2019).
- ⁵⁵ Y. H. Kwan, S. A. Parameswaran, and S. L. Sondhi, *Phys. Rev. B* **101**, 205116 (2020).
- ⁵⁶ A. Valsaraj, L. F. Register, E. Tutuc, and S. K. Banerjee, *Journal of Applied Physics* **120**, 134310 (2016).
- ⁵⁷ R. Bistritzer and A. H. MacDonald, *Proceedings of the National Academy of Sciences* **108**, 12233 (2011).
- ⁵⁸ L. A. Gonzalez-Arraga, J. L. Lado, F. Guinea, and P. San-Jose, *Phys. Rev. Lett.* **119**, 107201 (2017).